ON THE ROLE OF REVERSE CURRENT ON THE HARD X-RAY PRODUCTION IN SOLAR FLARES AND TIME-LAGS BETWEEN HIGH- AND LOW-ENERGY PHOTONS

RANJANA BAKAYA, S. A. CHASTI

Department of Physics, Regional Engineering College, Srinagar, India

and

R. R. RAUSARIA*

Indian Institute of Astrophysics, Kodaikanal, India

(Received 11 October, 1991)

Abstract. The evolution of energy and angular distributions of electrons has been studied accounting for the reverse current effect by combining analytically treated small angle multiple scatterings with large angle Monte-Carlo calculations. Reverse current and potential variations as function of column density have been computed. It is found that the reverse current decreases steeply with increase in electron energy. However, it becomes significant for low-energy electrons. By use of these distributions and bremsstrahlung cross-section, the X-ray energy spectrum has been calculated. The nature of the resulting X-ray spectrum integrated over all column depths is similar to the one without reverse current. The time-lag between high- and low-energy photon production has been calculated. It is found that there is a small difference between time-lags as function of observation angles. This fact can be used to test the validity of the beamed thick target model.

1. Introduction

The hard X-ray emitted during flares provide the most direct information about the accelerated energetic electrons. The X-ray energy spectrum above 10 keV is in most cases consistent with a power law of the differential photon flux (Kane and Anderson, 1970). The hard X-radiation is believed to be mainly due to bremsstrahlung in collisions between energetic electrons and the ions of the solar atmosphere. Electrons with power-law energy spectrum can produce power-law photon spectrum usually observed and, therefore, this fact was regarded as an evidence of the non-thermal origin of the solar hard X-rays (Takakura, 1966; Holt and Cline, 1968; Holt and Ramaty, 1969).

For non-thermal hard X-rays thin and thick target models have been proposed. In the thin target approximation, the electron escape time is much smaller than the energy loss time (low-density source) and the electrons lose only a small part of their energy in the medium (Brown and Melrose, 1977; Kane *et al.*, 1980). The X-ray flux depends on the instantaneous electron number and the X-ray yield is low. On the other hand, in the 'thick target' beam model the energetic electron beams are injected in high-density medium, the energy loss time is very short and a continuous electron injection is required to reproduce the observed duration of the X-ray burst. The instantaneous electron

* Presently on leave from Regional Engineering College, Srinagar, India.

Astrophysics and Space Science **195**: 401–412, 1992.

spectrum is different from the injection spectrum and the X-ray flux depends on the injectum spectrum (Brown, 1971, 1972). The X-ray yield is higher than in the 'thin target' case. The electron energy content is comparable to the total energy released during the flare and the large electron beam currents induced demand that a neutralizing reverse current be rapidly established among the ambient electrons (Brown and Melrose, 1977; Heyvaerts, 1981). The effect of reverse current accounting for multiple scattering has not been studied in detail on the production of the X-ray. Therefore, in this work we have studied in detail the generation of reverse current at different depths in the Sun atmosphere and have calculated the resulting change in the electron energy and angular distribution. By use of these distributions the X-ray energy spectrum and time-lag between low- and high-energy photons has been computed and the results are compared with the observations.

2. Calculation of X-Ray Flux

Following the method of Haug *et al.* (1985) after taking into consideration of thick target bremsstrahlung model in its simplest version (Brown, 1971; Syrovatskii and Shmeleva, 1972; Emslie, 1980, Leach and Petrosian, 1981), the photon flux produced by electrons in a fixed direction is given by

$$J(\vartheta) = n_{\mathrm{H}} \int_{1+k}^{\varepsilon} \mathrm{d}\varepsilon\, \mathrm{d}(\cos\alpha) \int_{0}^{2\pi} \mathrm{d}\phi g(\alpha)\, \frac{\mathrm{d}^2\sigma}{\mathrm{d}(h\nu)\,\mathrm{d}\Omega}\, f(\varepsilon)\, v(\varepsilon)\,, \tag{1}$$

where ε is the electron energy in units of rest mass energy mc^2; $K = h\nu/mc^2$, the photon energy in the same units; $\mathrm{d}^2\sigma/\mathrm{d}(h\nu)\,\mathrm{d}\Omega$, differential bremsstrahlung cross-section; $f(\varepsilon)$, the electron distribution; $g(\alpha)$, the electron angular distribution; ϑ, the angle between the vertical direction and line-of-sight; θ, the angle between the electron and photon directions.

In the presence of a magnetic field the electron direction will change continuously due to spiralling. For any observation the angle ϑ is actually fixed. The relation between ϑ and the electron incidence angle α, the angle θ, and the azimuth angle ϕ of the electron relative to vertical direction is given as

$$\cos\vartheta = \cos\alpha\cos\theta + \sin\alpha\sin\theta\cos\phi\,. \tag{2}$$

Usually the energy spectrum of the electrons is deduced from measured X-ray spectrum and as already given in the Introduction above 10 keV is taken to be of a power-law form. Here we consider initially monoenergetic incident beams, i.e., electrons having 60, 100, and 300 keV energy, characterized by a velocity vector $\mathbf{v}$ (in Z-direction towards the chromosphere from corona). The choice of monoenergetic beams are justified by the fact that the power-law shape of the energy distribution can be obtained by giving suitable weights to the monoenergetic electrons. The components of $\mathbf{v}$ in a coordinate system with Z-axis are $\sin\alpha\cos\phi$, $\sin\alpha\sin\phi$, and $\cos\alpha$, where α is the incidence angle

with respect to the vertical direction and becomes the pitch angle in presence of a magnetic field. We take the electrons directed towards the chromosphere from the acceleration site situated in the corona at 0°, 30°, and 60° incidence angles and follow their trajectory by combining small angle scattering using analytical treatment with a large angle collision using Monte-Carlo calculations. The details of the method are given in Haug *et al.* (1985). By this procedure we determine the electron energy and angular distributions at different column densities (i.e., heights) in the solar atmosphere. The energy and angular distributions become broader and diffuse with the increase in the depth of penetration for all the incidence angles and energies of electrons. The number of back-scattered electrons, however, increases for higher incidence angles. The differential bremsstrahlung cross-section in the Born approximation following Sauter (1934) multiplied by the Coulomb correction (Elwert, 1939) is used in the present computation. It is given in Elwert and Haug (1971) as Equation (6). In this equation the second term in parenthesis should read $(\varepsilon^2 + 1 + \frac{1}{2}\varepsilon p' \cos\theta)$. If we integrate over all the emissions angles one gets the total bremsstrahlung flux as function of energy only.

3. Effect of Reverse Current on Electron Distribution

It is now generally recognized (Hoyng, 1977; Hoyng *et al.*, 1976, 1978; Brown and Melrose, 1977; Knight and Sturrock, 1977; Colgate, 1978) that the large beam currents required by non-thermal electron beam models of hard X-ray bursts and chromospheric heating during solar flares demand that a neutralization reverse current be rapidly established among the ambient electrons. This current is driven by the beam-induced electric and magnetic fields which, if a reverse current did not arise, would rapidly gain energies exceedingly that of the flare itself.

Knight and Sturrock (1977) examined the behaviour of this reverse current and its associated energy distribution rate with depth, and deduced that it was likely to play an important role in the impulsive heating of the preflare chromosphere. This conclusion is in accordance with the statement made by Spicer *et al.* (1979) that Ohmic losses are the dominant loss mechanisms of most electron beams in the rarified gases. However, Knight and Sturrock (1977) admit that during the post-flare period where coronal temperatures have significantly risen, reverse current Ohmic heating being inversally proportional to $T^{3/2}$ in the case of classical resistivity (Spitzer, 1962) will not be as important as it is during the impulsive phase of event. Furthermore, they neglect collisional scattering of the beam electrons in their beam dynamical equations. This overestimates the beam current in the target and also renders their model unphysical, since a highly collimated beam is, in the absence of collisions, highly unstable (Shapiro and Shevchenko, 1968).

Emslie (1980) examined a model problem with a non-thermal source (Somov and Syrovatskii, 1976) of fast electrons including the reverse current electric field and found that it could lead to significant changes of intensity and polarization of X-rays. Diakonov and Somov (1988) have included the reverse current electric field in the cold plasma for the case of an abrupt transition layer between the hot plasma of a flare and

the cold plasma in the solar atmosphere. They have shown that it is impossible to solve the reverse current problem self-consistently without taking collisions into account.

The theoretical modelling of collisional losses suffered by a beam of electrons in passage through a hydrogen chromosphere is well established (e.g., Brown, 1974; Lin and Hudson, 1976; or Emslie, 1978). However, the evaluation of the expected energy deposition at chromospheric levels from such a beam and comparison with the radiated energies at these depths indicates either that the hard X-rays commonly attributed to non-thermal electron beams are, in fact, predominantly thermal in origin (Chubb, 1971; Brown, 1974; Brown *et al.*, 1979; Colgate, 1978; Cranell *et al.*, 1978; Emslie and Brown, 1980) or that the electrons are somehow coronally confined. It is conceivable that Ohmic losses from the beam may result in such a confinement, since in the low-density corona such losses are more important than those due to direct collisions of the beam with the ambient plasma.

Since the ambient electrons are preferentially (over protons) heated both by collisional and Ohmic processes, the ion temperature T_i will be much less than T_e especially in regions of low density, where time-scales for temperature equilibrium are very long (Spitzer, 1962). The beam's behaviour will be governed by both collisional and Ohmic (i.e., reverse current) processes plus losses to plasma wave generation if the return current become unstable (see Brown *et al.*, 1979). These produce changes in the beam electron energy E and momentum $m_e v$ (where m_e is the electron mass) given by

$$\frac{\mathrm{d}E}{\mathrm{d}N} = \left(\frac{\mathrm{d}E}{\mathrm{d}N}\right)_C + \left(\frac{\mathrm{d}E}{\mathrm{d}N}\right)_r \tag{3}$$

and

$$\frac{\mathrm{d}V_z}{\mathrm{d}N} = \left(\frac{\mathrm{d}V_z}{\mathrm{d}N}\right)_C + \left(\frac{\mathrm{d}V_z}{\mathrm{d}N}\right)_r , \tag{4}$$

where N is the overlying column density (cm^{-2}) of the atmosphere, and subscripts Z, C and r refer to the vertical component and to collisional and reverse current losses, respectively.

In order to calculate this reverse current we have used Ohm's law. According to Ohm's law, the electric field E which generates reverse current is given as

$$\mathbf{J} = \sigma \mathbf{E} , \tag{5}$$

where $\mathbf{J}$ is the conduction current density and σ is the conductivity. This conduction current density $\mathbf{J}$ of this field with density n/cm^3 is

$$\mathbf{J} = ne\mathbf{v} , \tag{6}$$

where the electron density $\mathbf{v}$ is given by

$$\mathbf{v} = 5.95 \times 10^5 E \ \mathrm{m\ s}^{-1} .$$

By use of Equations (5) and (6), the electric field is

$$\mathbf{E} = \frac{ne\mathbf{v}}{\sigma} \,. \tag{7}$$

The conductivity of a medium with temperature T is

$$\sigma = \frac{T^{3/2}}{\ln \Lambda} (1.52 \times 10^{-2}) \text{ mhos m}^{-1} \,. \tag{8}$$

The numerical expression for Λ is given by

$$\Lambda = 1.24 \times 10^{7} (T^3/n) \,, \quad n \text{ is cm}^{-3} \,.$$

If we use Equations (7) and (8), we have calculated the change in the energy of electrons in presence of reverse electric field. Figures 1(a) and 1(b) show the variation of electron energy distribution accounting for reverse electric field. These figures have been plotted for incident electron energies 30 and 60 keV for incidence angle 0° and 30°. A look at the figure shows that electron flux decreases with the decrease in electron energy. The decrease in the flux value is due partly to the loss of some of its energy in collisions with ambient plasma while moving downwards (i.e., in forward direction) and partly on account of the loss of energy due to reverse current. These two effects together account for larger decrease in electron energy. By use of the above equation and electron distributions we have calculated the current which develops due to the presence of

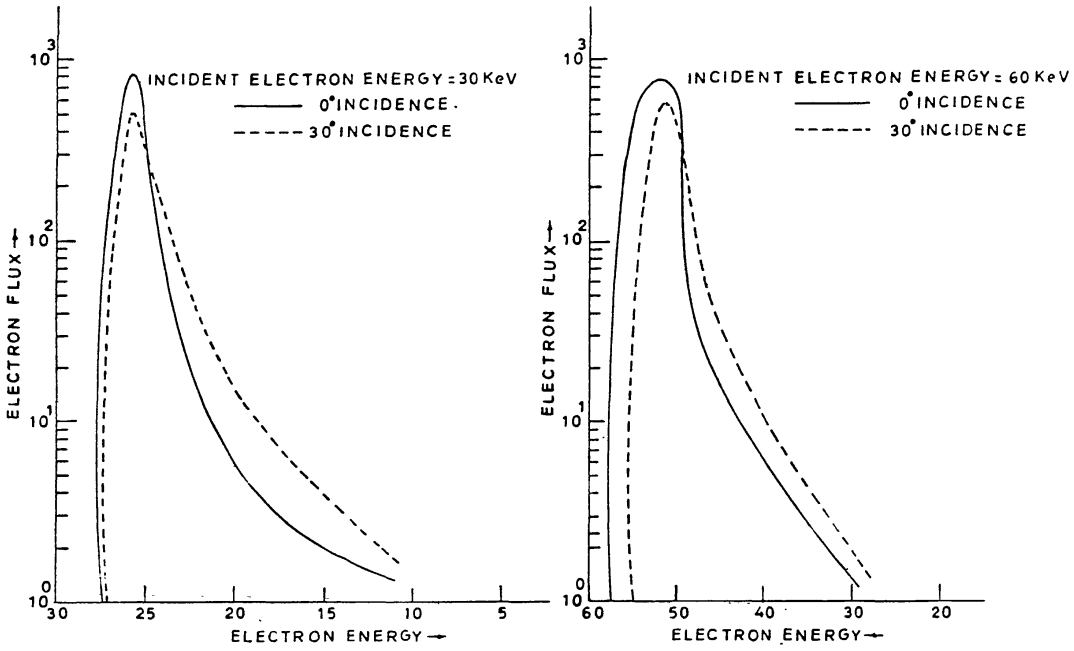

Fig. 1a. Variation of electron flux with electron energy accounting for reverse current effect for 30 keV energy incident at 0° and 30°.

Fig. 1b. Same as Figure 1(a) but for 60 keV incident energy.

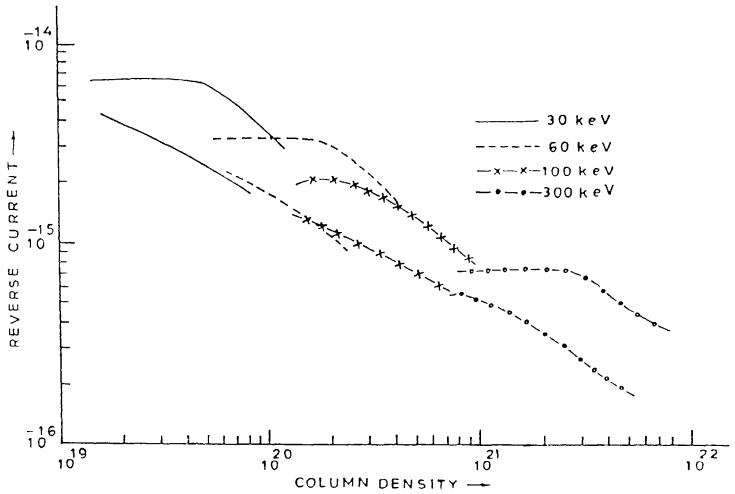

Fig. 2. Variation of reverse current with column density for 30, 60, 100, and 300 keV electron beams incident at 0° (upper line) and 60° (lower line).

reverse electric field. This reverse current is plotted against column density for 30, 60, 100, and 300 keV incident electron beams in Figure 2 at 0° and 60° incidence. From the figure we find that initially, i.e., at lower column densities, the current is higher and decreases with the increase in column density. At lower column densities, the background particle density is small resulting in few number of collisions so that the electrons continue to move in forward direction without getting trapped. This effect manifests itself in the form of an increase in current. As column density increases, ambient particle density also increases resulting in more collisions, so electron velocity is reduced continuously resulting in decrease in current. From the figure we also note that with the increase in incident electron energy, current increases. If we use the expression for σ given by Equation (8) we have calculated conductivity for the reverse current field which we have plotted in Figure 3 as a function of column density for incident electron energies 30, 60, 100, and 300 keV with 0° and 60° incidence. Conductivity being a function of current decreases with the increase in column density.

Figure 4 shows the variation of reverse current as function of potential for 30, 60, and 100 keV electron beams with 0° and 30° incidence. From the figure we see that in the beginning, the effect of reverse current is appreciable, i.e., at lower column densities where potential is small, then it decreases smoothly.

We have also calculated the potential of the reverse electric field using the familiar equation $E = -\nabla V$. Figure 5 shows the variation of potential as a function of column density for electron energies 30, 60, 100, and 300 keV with 0° and 60° incidence. The potential increases rapidly at lower column densities and then rises smoothly.

4. Results and Discussion

By use of the bremsstrahlung cross-section given in Elwert and Haug (1971) and the electron distribution function $f(\varepsilon)$ and $g(\alpha)$ described in previous section, we have

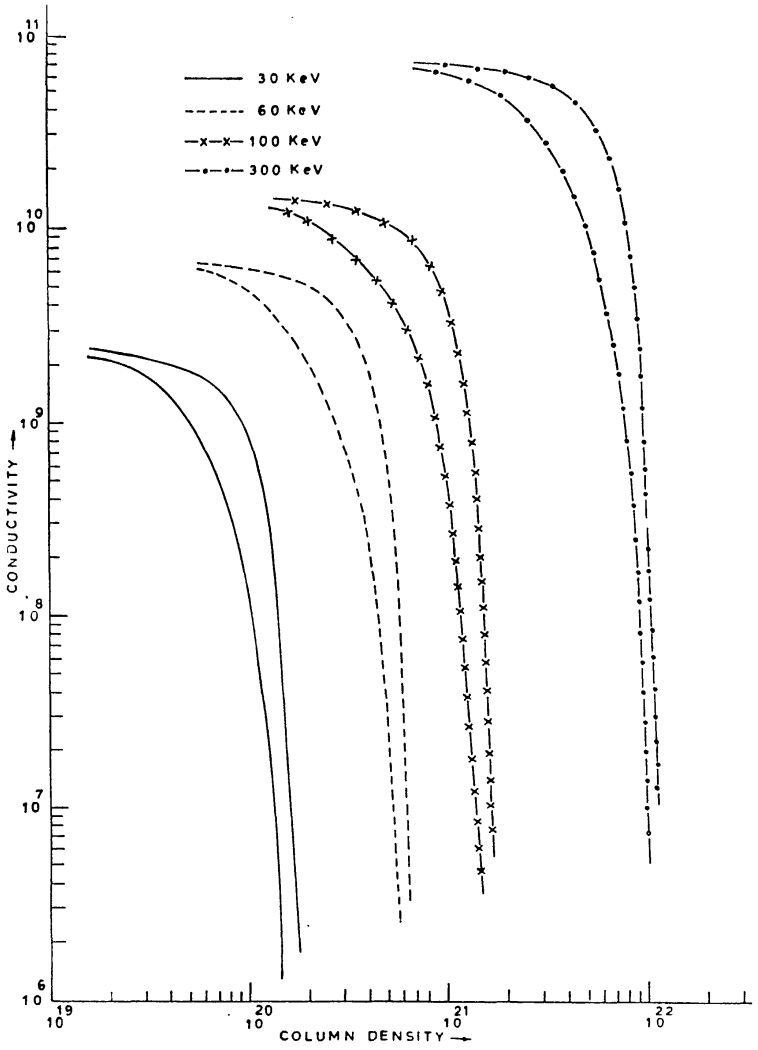

Fig. 3. Variation of conductivity with column density for 30, 60, 100, and 300 keV electron beam incident at 0° (upper line) and 60° (lower line).

computed the energy spectra of the X-rays. The X-ray energy spectra integrated over all depths is plotted in Figure 6. The nature of integrated spectra is similar to that in absence of reverse current. The shape of calculated integrated spectrum corresponds well with observed energy spectrum obtained from PVO and ISEE-3 spacecraft (Figure 1 of Kane *et al.*, 1980).

The variations of photon flux as a function of column density (for 30, 45, 60, and 90 keV photons) are plotted in Figures 7(a) and 7(b). These figures show that the X-ray production maximizes at different column densities for various electron energies incident at fixed angle. Furthermore, we note that the photon production corresponding to each spot value of the energy maximizes at lower column density for 60° incidence compared to 30° and 0° electron incidences. The width of the height distribution for a particular photon energy becomes broader with the increase in electron incidence

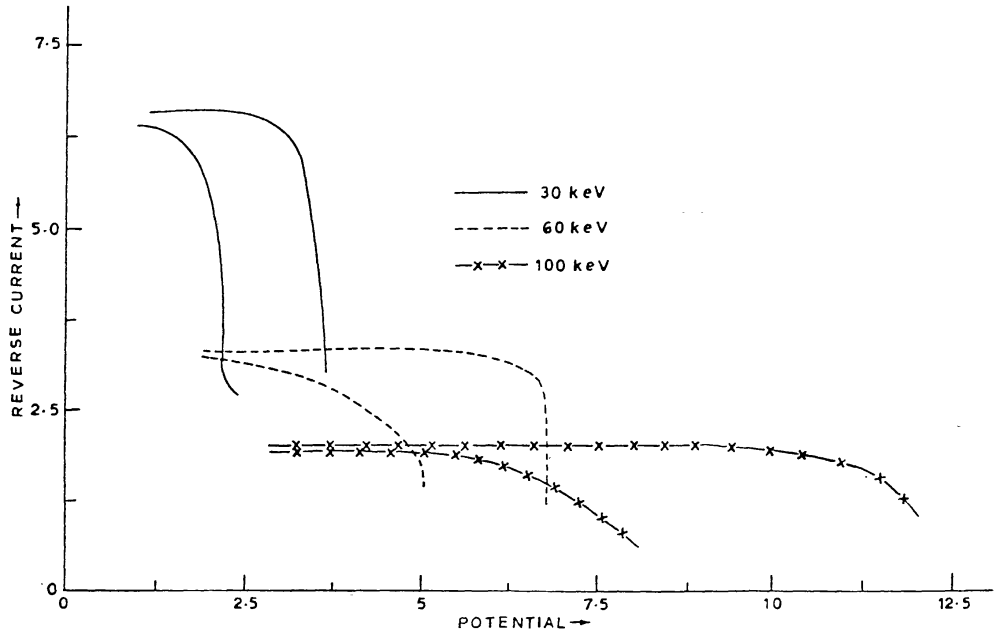

Fig. 4. Variation of reverse current with potential for 30, 60, and 100 keV electron beams incident at 0° (upper line) and 30° (lower line).

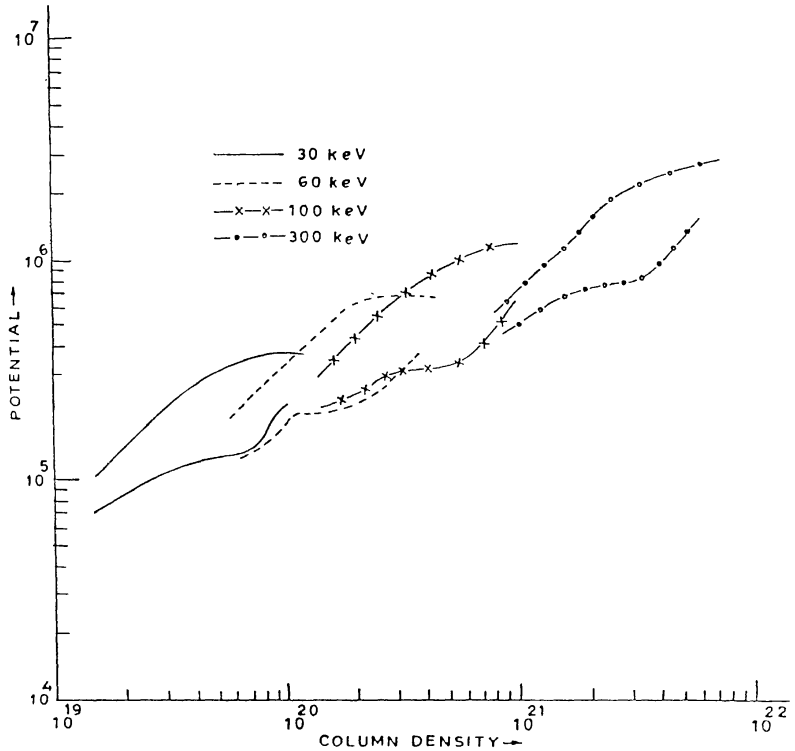

Fig. 5. Variation of potential with column density for 30, 60, 100, and 300 keV electron beams incident at 0° (upper lines) and 60° (lower lines).

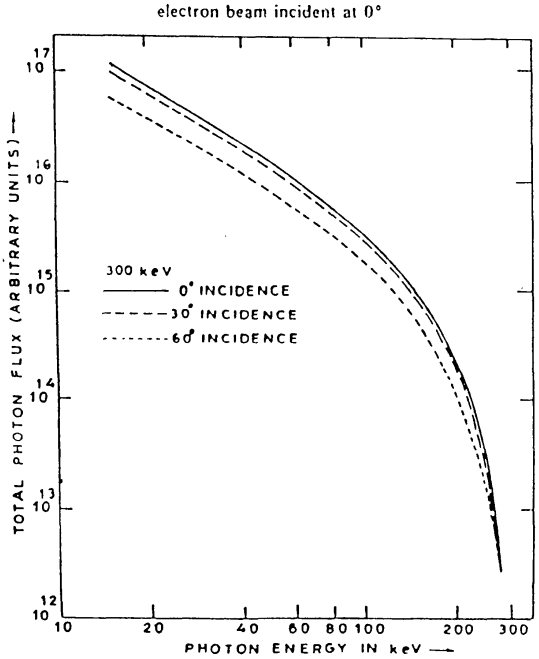

Fig. 6. X-ray flux spectra integrated over all column densities, i.e., spatially-integrated X-ray energy spectrum for a 300 keV electron beam incident at 0°, 30°, and 60°.

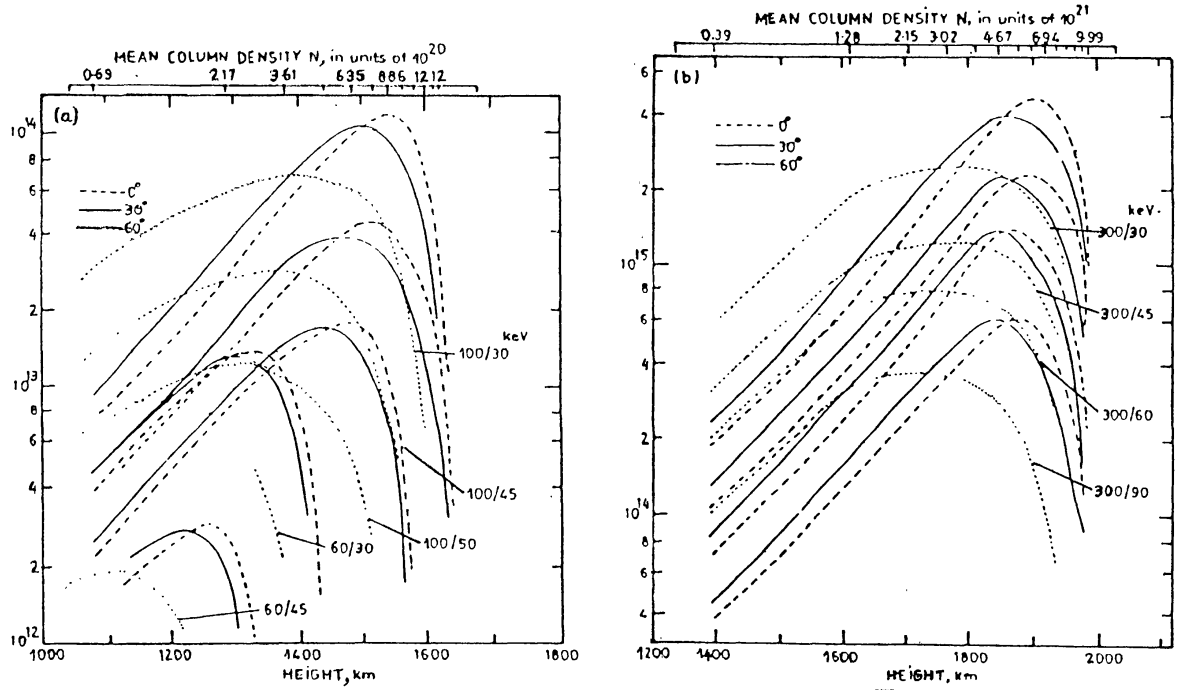

Fig. 7a. Variation of photon flux with height for 0°, 30°, and 60° electron incidence angles (the incident electron energies are 60 and 100 keV and 100/30 on the curve signifies 100 keV electrons and 300 keV photon energy).

Fig. 7b. Same as Figure 7(a) but for the incident electron energy 300 keV.

angles. For 60° electron incidence, the distribution of photon flux with height becomes broadened and does not show much pronounced peak. These figures also show that the width of the X-ray profile becomes smaller with increase in photon energy and for electron incidence angles approaching 0°.

If we follow the method given in Koul *et al.* (1987), we have converted the height profile of X-rays into time profiles. From the study of time-profile curve we find that the peak for high-energy photons appear earlier than that for low-energy photons (Figure 8). If we use this figure, we have calculated the time-lag between high- and low-energy photons. It is plotted in Figure 9(a). From the figures we find that time is more if the incident electron energy is less. The time lag decreases with the increase in electron energy. This can be explained by the fact that high-energy electrons penetrate deeper into the atmosphere and lose energy quickly. The variation of time-lag as function of photon energy for two observation angles 50° and 90° are plotted in Figure 9(b). The nature of curves in both cases remains the same. There is a slight difference in the magnitude of time-lag for 50° and 90° observation angles. This fact could be used to test the beamed thick target model. Millisecond time variations in hard X-ray profile has already been measured by Kiplinger *et al.* (1983). By use of two satellites separated in heliographic longitude, it is, in principle, possible to measure the evolution of X-ray pulse at different observation angles. From this, time-lag between high- and low-energy photons can be deduced. In conclusion we can say that reverse current plays an important role on the hard X-ray production at lower column density and the time difference between high- and low-energy electrons can be used to test the validity of beamed thick target model.

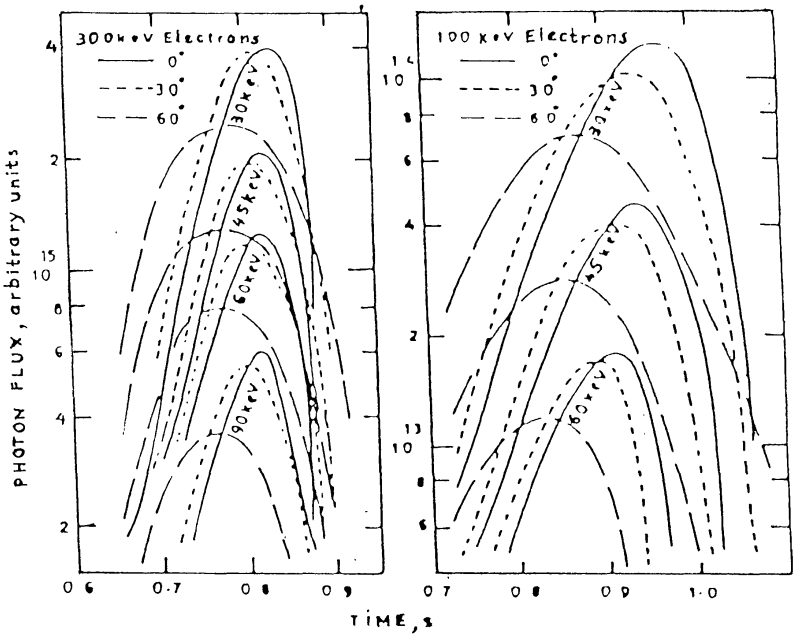

Fig. 8. Time variation of photon flux for 100 and 300 keV electron energies with incidence angles, 0°, 30°, and 60°.

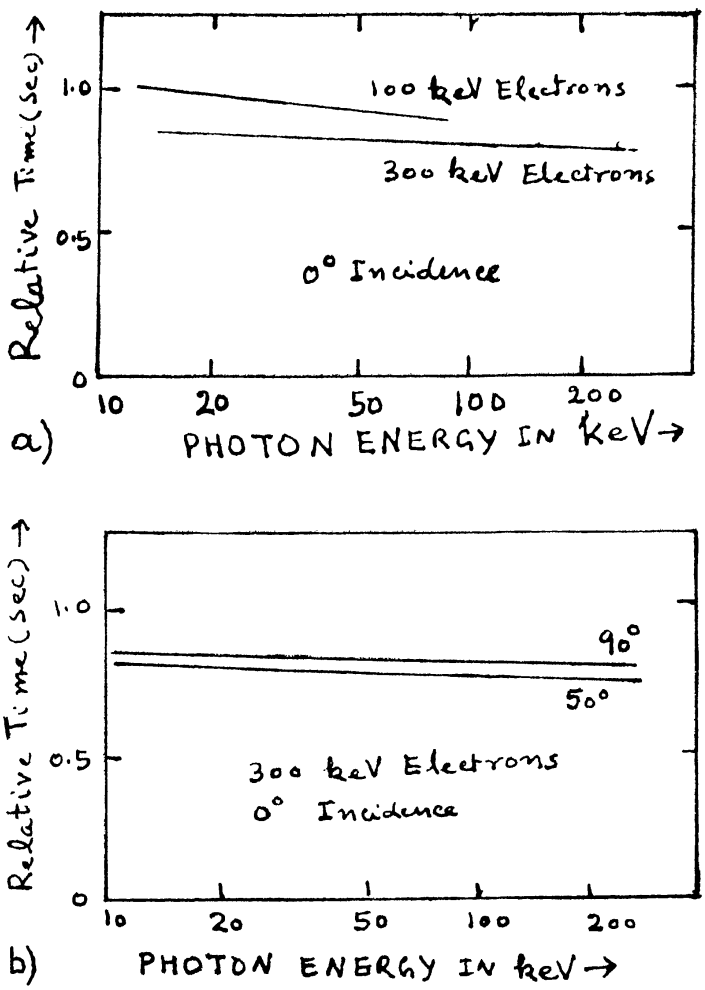

Fig. 9a. Variation of relative peak time(s) as function of photon energy.

Fig. 9b. Relative peak time and its variation with photon energy for fix observation angles.

References

Brown, J. C.: 1971, *Solar Phys.* **25**, 158.
Brown, J. C.: 1972, *Solar Phys.* **26**, 441.
Brown, J. C.: 1974, in G. A. Newkirk (ed.), 'Coronal Disturbances', *IAU Symp.* **57**, 395.
Brown, J. C. and Melrose, D. B.: 1977, *Solar Phys.* **52**, 117.
Brown, J. C., Melrose, D. B., and Spicer, D. S.: 1979, *Astrophys. J.* **228**, 592.
Chubb, T. A.: 1970, in E. R. Dyer (ed.), *Solar Terrestrial Physics*, Part I, D. Reidel Publ. Co., Dordrecht, Holland.
Colgate, S. A.: 1978, *Astrophys. J.* **221**, 1068.
Cranell, C. J., Frost, K. J., Matzler, C., Ohki, K., and Saba, J. L.: 1978, *Astrophys. J.* **223**, 620.
Diakonov, S. V. and Somov, B. V.: 1988, *Solar Flare Plasma Physics,* Izmiran, Moscow.
Elwert, G.: 1939, *Ann. Phys.* **34**, 178.
Elwert, G. and Haug, E.: 1971, *Solar Phys.* **20**, 413.
Emslie, A. G.: 1978, *Astrophys. J.* **224**, 241.
Emslie, A. G.: 1980, *Astrophys. J.* **235**, 1055.
Emslie, A. G. and Brown, J. C.: 1980, *Astrophys. J.* **237**, 1015.
Haug, E., Elwert, G., and Rausaria, R. R.: 1985, *Astron. Astrophys.* **146**, 159.

Heyvaerts, J.: 1981, in E. R. Priest (ed.), *Solar Flare Magnetohydrodynamics*, Gordon and Breach, New York, p. 429.
Hoyng, P.: 1977, *Astron. Astrophys.* **55**, 23.
Hoyng, P., Brown, J. C., and Van Beek, H. E.: 1976, *Solar Phys.* **48**, 197.
Hoyng, P., Knight, J. W., and Spicer, D. S.: 1978, *Solar Phys.* **58**, 139.
Holt, S. S. and Cline, T. L.: 1968, *Astrophys. J.* **154**, 1027.
Holt, S. S. and Ramaty, R.: 1969, *Solar Phys.* **8**, 119.
Kahler, S. W.: 1975, in S. R. Kane (ed.), 'Solar Gamma, K and EUV Radiation', *IAU Symp.* **68**, 211.
Kane, S. R. and Anderson, K. A.: 1970, *Astrophys. J.* **162**, 1003.
Kane, S. R., Anderson, K. A., Evans, W. D., Klebesadel, R. W., and Laros, J. G.: 1980, *Astrophys. J.* **239**, L85.
Kiplinger, A. L., Dennis, B. R., Emslie, A. G., Frost, K. J., and Orig, L. E.: 1983, *Astrophys. J.* **265**, L91.
Knight, J. A. and Sturrock, P. A.: 1977, *Astrophys. J.* **218**, 306.
Koul, P. K., Rausaria, R. R., and Khose, P. N.: 1987, *Solar Phys.* **108**, 739.
Leach, J. and Petrosian, V.: 1981, *Astrophys. J.* **251**, 781.
Lin, R. P., Mewaldt, R. A., and Van Hollebeke, M. A. I.: 1982, *Astrophys. J.* **253**, 949.
Sauter, F.: 1934, *Ann. Phys.* **20**, 404.
Shapiro, V. D. and Shevchenko, V. J.: 1968, *Soviet Phys. JETP* **27**, 635.
Somov, B. V. and Syrovatskii, S. I.: 1976, *Soviet Phys. Usp.* **19**, 813.
Spicer, D. S., Tidman, D. A., and Hubbard, R. F.: 1979, *Nucl. Fusion.*
Spitzer, L.: 1962, *Physics of Fully Ionized Plasma,* John Wiley and Interscience Publ., New York.
Syrovatskii, S. I. and Shmeleava, C. P.: 1972, *Astron. Zh.* **49**, 334.
Takakura, T. and Kai, K.: 1966, *Publ. Astron. Soc. Japan* **18**, 57.